Effect of base-flow variation in noise amplifiers: the flat-plate boundary layer

Luca Brandt[1]†, Denis Sipp[2], Jan O. Pralits[3] and Olivier Marquet[2]

[1] Linné Flow Centre, KTH Mechanics, S-100 44 Stockholm, Sweden
[2] ONERA/DAFE, 8 rue des Vertugadins, 92190 Meudon, France
[3] DIMEC, University of Salerno, Via Ponte don Melillo, 84084 Fisciano (SA), Italy

Non-modal analysis determines the potential for energy amplification in stable flows. The latter is quantified in the frequency domain by the singular values of the resolvent operator. The present work extends previous analysis on the effect of base-flow modifications on flow stability by considering the sensitivity of the flow non-modal behaviour. Using a variational technique, we derive an analytical expression for the gradient of a singular value with respect to base-flow modifications and show how it depends on the singular vectors of the resolvent operator, also denoted the optimal forcing and optimal response of the flow. As an application, we examine zero-pressure-gradient boundary layers where the different instability mechanisms of wall-bounded shear flows are all at work. The effect of the component-type non-normality of the linearized Navier–Stokes operator, which concentrates the optimal forcing and response on different components, is first studied in the case of a parallel boundary layer. The effect of the convective-type non-normality of the linearized Navier–Stokes operator, which separates the spatial support of the structures of the optimal forcing and response, is studied in the case of a spatially evolving boundary layer. The results clearly indicate that base-flow modifications have a strong impact on the Tollmien–Schlichting (TS) instability mechanism whereas the amplification of streamwise streaks is a very robust process. This is explained by simply examining the expression for the gradient of the resolvent norm. It is shown that the sensitive region of the lift-up (LU) instability spreads out all over the flat plate and even upstream of it, whereas it is reduced to the region between branch I and branch II for the TS waves.

Key words: boundary layer receptivity, control theory

1. Introduction

Unstable open flows can be classified into two distinct classes according to the linear evolution of perturbations in space and time (e.g. Huerre & Rossi 1998): noise amplifiers and hydrodynamic oscillators. If the perturbations initially amplified eventually decay in time or are convected away (usually downstream of the disturbance source, so that the flow returns to its basic state), then the flow behaves as a noise amplifier. These flows are sensitive to external perturbations and

† Email address for correspondence: luca@mech.kth.se

the characteristics of the latter determine the type of waves amplifying in the flow. Spatially developing jets or attached boundary layers are prototypes of noise amplifiers. Oscillator flows, on the other hand, display an intrinsic dynamics: they beat at a well-defined frequency, the features of the amplifying perturbations are determined solely by the control parameters and do not depend on external noise. The flow past a cylinder is probably the most classic example of an oscillator. Oscillators and amplifiers are related to different stability properties. In a local approach, an absolutely unstable flow is a necessary condition for an oscillator-type behaviour while an absolutely stable but convectively unstable flow relates to a noise amplifier. In a global approach, unstable flows coincide with oscillators while globally stable flows behave as noise amplifiers when governed by non-normal operators.

Analysis of normal-mode solutions is sufficient to investigate the stability of a given flow configuration at large times. The least stable among the flow eigenvalues provides this information. However even stable flows can undergo significant perturbation energy growth owing to the non-normality of the linearized Navier–Stokes equations. To assess the energy growth of stable flows, a non-modal or input–output approach is therefore required (Schmid & Henningson 2001). This type of analysis can be carried out in the time or frequency domain. In the first case, the aim is initial conditions yielding the largest possible energy growth over a finite time horizon (Butler & Farrell 1992; Reddy & Henningson 1993) whereas in the second case the aim is the largest possible response to time-periodic external forcing (see also Farrell & Ioannou 1996; Jovanovic & Bamieh 2005): both approaches reflect the non-normality of the governing operator and yield a measure quantifying energy amplifications in the flow, the *singular values of the governing operator*.

Besides the correct tools and concepts, when theoretically studying the stability of fluid systems, a relevant definition of a base flow is the first important step. In the review by Chomaz (2005), it is explained how small perturbations of non-normal operators may displace the eigenvalues in a significant manner. These perturbations will have a larger impact if they occur in the overlap region between the adjoint and direct eigenmodes. Bottaro, Corbett & Luchini (2003) examined the worst case, i.e. the change in base flow with the most destabilizing effect on the eigenvalues for the plane Couette flow. Such base-flow variations were interpreted as differences between the laboratory flow and its ideal, theoretical counterpart. Later studies considered transition to turbulence initiated by base-flow defects (see e.g. Gavarini, Bottaro & Nieuwstadt 2004). The concept of sensitivity to base-flow modifications of a given eigenvalue, introduced for parallel shear flows in Bottaro *et al.* (2003), was extended to the global approach by Marquet, Sipp & Jacquin (2008) and Pralits, Brandt & Giannetti (2010). In order to identify the 'engine' of the instability Giannetti & Luchini (2007) determined the sensitivity of the eigenvalue to a spatially localized feedback. Global instabilities are generated by a self-exciting mechanism and regions with a larger sensitivity play the same role as the 'wavemaker' of the asymptotic theory in slowly developing flows (Chomaz, Huerre & Redekopp 1991).

The objective of the present paper is to extend similar concepts to the case of noise amplifiers. The starting point of the analysis is that the essential dynamics of the flow cannot be captured by the eigenvalues of the governing operator, which characterize well the behaviour of hydrodynamic oscillators. Therefore we analyse the singular values of the system (Sipp *et al.* 2010), thus centring our investigation on the non-modal behaviour of the flow. The central concept in this paper is the *sensitivity of the singular values with respect to base-flow modifications*. This type of analysis also includes modal stability, in some sense: if a mode becomes unstable, the

singular value becomes infinite at the neutral point. Particular attention will be paid to the different sources of non-normality of the linearized Navier–Stokes operator. As introduced by Chomaz (2005) and Marquet *et al.* (2009) in the context of unstable eigenvalues, this operator displays two sources of non-normality: the *component-type non-normality*, which concentrates the direct and adjoint eigenmodes on different components of the velocity field; and the *convective-type non-normality* which separates the spatial support of the eigenmodes, typically upstream for the adjoint eigenmode and downstream for the direct eigenmode. As shown by Monokrousos *et al.* (2010), similar features are also observed for the singular vectors of the equations governing the behaviour of linear perturbations in boundary layer flows. We will analyse how *the sensitivity of the singular value to base-flow modifications* depends on the type of non-normality.

As an application, we focus on the Blasius boundary layer, where the traditional instability mechanisms observed in wall-bounded shear flows are present. In these flows, the non-modal behaviour stems from the lift-up (LU) and Orr mechanisms and from the convective dynamics of the Tollmien–Schlichting (TS) waves. The LU mechanism (Landahl 1980) is associated with the component-wise transfer of energy from the cross-stream velocity components (streamwise vorticity) to the streamwise velocity, the component-wise non-normality. It is most effective for low-frequency streamwise-elongated perturbations and is manifested in the appearance of high- and low-speed streaks alternating in the spanwise direction. The Orr mechanism is also related to component-wise transfer of energy and is most evident for two-dimensional waves that can gain some energy by leaning against the mean shear (Farrell 1988).

The article proceeds as follows. First (§ 2), we introduce the resolvent, its singular-value decomposition and the sensitivity of a singular value to base-flow modifications. In § 3, we analyse the case of a parallel boundary layer, where only the component-type non-normality is at play. First conclusions will be drawn concerning the sensitivity of the LU and TS instabilities. The spatially evolving boundary layer, where both the convective-type non-normality and the component-type non-normality are present, is examined in § 4. The paper ends with a discussion of the main results and some concluding remarks (§ 5).

2. Gradient of the resolvent operator

2.1. *Optimal forcing and eigenvalue problem*

We consider the evolution of small-amplitude perturbations about a steady base flow in the presence of a divergence-free forcing term $\boldsymbol{f}'$. Let x, y and z be the streamwise, cross-stream and spanwise coordinates with $\boldsymbol{U} = (U, V, W)$ and $\boldsymbol{u}' = (u', v', w')$ the streamwise, cross-stream and spanwise components of the base flow and perturbation respectively. The linearized equations describing the evolution of perturbations are

$$\partial_t \boldsymbol{u}' + (\boldsymbol{U} \cdot \boldsymbol{\nabla})\boldsymbol{u}' + (\boldsymbol{u}' \cdot \boldsymbol{\nabla})\boldsymbol{U} = -\boldsymbol{\nabla} p' + Re^{-1}\nabla^2 \boldsymbol{u}' + \boldsymbol{f}', \qquad (2.1)$$

$$\boldsymbol{\nabla} \cdot \boldsymbol{u}' = 0, \qquad (2.2)$$

where p denotes pressure and Re Reynolds number.

To investigate the linear stability of a stable flow, e.g. a spatial boundary layer that acts as an amplifier of external noise, we assume the forcing term to be harmonic in time with a real forcing frequency $\omega = 2\pi/T$ and a complex spatial structure $\boldsymbol{f} = (f, g, h)^{\mathrm{T}}$, $\boldsymbol{f}' = \boldsymbol{f} e^{i\omega t}$. A similar decomposition is used for the flow perturbation, where $(\boldsymbol{u}, p)$ is the spatial distribution of the perturbation sustained by the forcing $\boldsymbol{f}$. In a compact form, the relation between the forcing and the velocity perturbation can be

formally written

$$\boldsymbol{u} = \mathscr{R}(\omega, \boldsymbol{U})\boldsymbol{f}, \quad \mathscr{R} = \mathscr{P}^{\mathrm{T}}\mathscr{S}(\omega, \boldsymbol{U})^{-1}\mathscr{P}, \quad \mathscr{S} = \mathrm{i}\omega\mathscr{M} + \mathscr{L}(\boldsymbol{U}). \quad (2.3)$$

Here $\mathscr{M} = \mathscr{P}\mathscr{P}^{\mathrm{T}}$ with $\mathscr{P}$ as the prolongation operator, $\mathscr{R}$ is the resolvent operator, and $\mathscr{S}$ and $\mathscr{L}$ define the linearized Navier–Stokes operator. The prolongation operator $\mathscr{P}$ acts on a velocity vector $\boldsymbol{u} = (u, v, w)^{\mathrm{T}}$ to give the velocity–pressure vector $\mathscr{P}\boldsymbol{u} = (u, v, w, 0)^{\mathrm{T}}$, while the extraction operator $\mathscr{P}^{\mathrm{T}}$ acts on a velocity–pressure vector $\boldsymbol{q} = (u, v, w, p)^{\mathrm{T}}$ to give the velocity vector $\mathscr{P}^{\mathrm{T}}\boldsymbol{q} = \boldsymbol{u}$. The stability operator $\mathscr{L}$ is defined as follow:

$$\mathscr{L} = \begin{pmatrix} \mathscr{C} - \mathscr{D} + \partial_x U & \partial_y U & \partial_z U & \partial_x \\ \partial_x V & \mathscr{C} - \mathscr{D} + \partial_y V & \partial_z V & \partial_y \\ \partial_x W & \partial_y W & \mathscr{C} - \mathscr{D} + \partial_z W & \partial_z \\ \partial_x & \partial_y & \partial_z & 0 \end{pmatrix}, \quad (2.4)$$

where $\mathscr{C} = U\partial_x + V\partial_y + W\partial_z$ is the convection operator and $\mathscr{D} = Re^{-1}(\partial_x^2 + \partial_y^2 + \partial_z^2)$ is the diffusion operator.

To measure the growth of the perturbation we choose the kinetic energy in the flow domain Ω, $E(\boldsymbol{u}) = \int_\Omega \boldsymbol{u}^H \boldsymbol{u}\, \mathrm{d}\Omega = (\boldsymbol{u}, \boldsymbol{u})$. The symbol ^{H} indicates the trans-conjugate and $(\boldsymbol{a}, \boldsymbol{b})$ denotes the inner product of two fields $\boldsymbol{a}$ and $\boldsymbol{b}$. The gain between the forcing $\boldsymbol{f}$ and the perturbation $\boldsymbol{u}$ is given by

$$G = \frac{(\boldsymbol{u}, \boldsymbol{u})}{(\boldsymbol{f}, \boldsymbol{f})} = \frac{(\mathscr{R}\boldsymbol{f}, \mathscr{R}\boldsymbol{f})}{(\boldsymbol{f}, \boldsymbol{f})} = \frac{(\mathscr{R}^\dagger \mathscr{R}\boldsymbol{f}, \boldsymbol{f})}{(\boldsymbol{f}, \boldsymbol{f})}, \quad (2.5)$$

where the last equality is obtained by introducing the operator $\mathscr{R}^\dagger$, the adjoint operator of the resolvent operator $\mathscr{R}$ with respect to the inner product introduced above. It is given by $\mathscr{R}^\dagger = \mathscr{P}^{\mathrm{T}}(\mathscr{S}^\dagger)^{-1}\mathscr{P}$, where $\mathscr{S}^\dagger$ is the adjoint linearized Navier–Stokes operator defined by $\mathscr{S}^\dagger = \mathrm{i}\omega\mathscr{M} + \mathscr{L}^\dagger$. Here

$$\mathscr{L}^\dagger = \begin{pmatrix} -\mathscr{C} - \mathscr{D} + \partial_x U & \partial_x V & \partial_x W & -\partial_x \\ \partial_y U & -\mathscr{C} - \mathscr{D} + \partial_y V & \partial_y W & -\partial_y \\ \partial_z U & \partial_z V & -\mathscr{C} - \mathscr{D} + \partial_z W & -\partial_z \\ -\partial_x & -\partial_y & -\partial_z & 0 \end{pmatrix}. \quad (2.6)$$

Let us now consider the eigenvalue problem

$$\mathscr{R}^\dagger \mathscr{R}\boldsymbol{f}_i = \sigma_i^2 \boldsymbol{f}_i. \quad (2.7)$$

Since the operator $\mathscr{R}^\dagger \mathscr{R}$ is symmetric, the eigenvalues are real and positive and the eigenvectors $\boldsymbol{f}_i$ are orthogonal with respect to the energy inner product. The set of eigenvectors $\{\boldsymbol{f}_i\}_{i \geqslant 1}$ (right singular vector of $\mathscr{R}$) thus forms an orthonormal basis of the forcing space if normalized so that $(\boldsymbol{f}_i, \boldsymbol{f}_i) = 1$. The perturbation $\boldsymbol{u}_i$, left singular vector of $\mathscr{R}$, induced by the forcing $\boldsymbol{f}_i$ is given by $\boldsymbol{u}_i = \mathscr{R}\boldsymbol{f}_i$. The optimal forcing $\boldsymbol{f}_1$ corresponds to the largest eigenvalue σ_1^2 of (2.7) and it maximizes the gain $G(\boldsymbol{f})$. The resolvent norm corresponds to the square-root of the largest eigenvalue σ_1^2 of (2.7), equivalent to the largest singular value of $\mathscr{R}$. In the following, we will use this quantity to measure the non-modal behaviour. It depends on the frequency ω, on the Reynolds number Re and on the base flow $\boldsymbol{U}$: $\sigma^2(\omega, Re, \boldsymbol{U})$. The optimal energy gains σ_i^2, optimal forcings $\boldsymbol{f}_i$ and optimal responses $\boldsymbol{u}_i$ will form the basis of the optimization procedure introduced here. Using Krylov-subspace methods, it is now

possible to compute the largest eigenvalues of system (2.7) (Monokrousos *et al.* 2010; Sipp *et al.* 2010), as well as of its counterpart in the time domain (Barkley, Blackburn & Sherwin 2008; Blackburn, Barkley & Sherwin 2008) for flows in more complex geometries.

2.2. *Sensitivity to generic base-flow modifications*

In this section we are interested in determining the sensitivity of any eigenvalue σ^2 to any base-flow modification $\delta U = (\delta U, \delta V, \delta W)$. For a small-amplitude base-flow variation, the eigenvalue variation $\delta \sigma^2$ can be written as

$$\delta \sigma^2 = (\nabla_U \sigma^2, \delta U), \tag{2.8}$$

where $(\cdot, \cdot)$ is the inner product defined above and $\nabla_U \sigma^2$ designates the sensitivity function to a modification of the base flow.

To obtain an analytical expression of this function we use a Lagrangian technique where the objective of the optimization is the eigenvalue σ^2 and the constraints are given by the eigenvalue problem (2.7) yielding the optimal non-modal behaviour. To do this, we first rewrite the eigen-problem (2.7) as

$$\mathscr{S}(U)q = \mathscr{P}f, \quad \mathscr{S}^\dagger(U)a = \mathscr{M}q, \quad \sigma^2 f = \mathscr{P}^T a \tag{2.9}$$

where U is the control variable and a is introduced to split the eigenvalue problem. This is necessary since we need to differentiate the resolvent with respect to the base flow and an explicit expression for the inverse of the system matrix, appearing in the resolvent operator, is not available. We introduce the Lagrange multiplier or adjoint variables $\{f^\dagger, q^\dagger, a^\dagger\}$ and define a Lagrangian function $\mathscr{K}(\{\sigma, f, q, a\}, \{f^\dagger, q^\dagger, a^\dagger\}, U)$

$$\mathscr{K} = \sigma^2 - (q^\dagger, \mathscr{S}(U)q - \mathscr{P}f) - (a^\dagger, \mathscr{S}^\dagger(U)a - \mathscr{M}q) - (f^\dagger, \sigma^2 f - \mathscr{P}^T a). \tag{2.10}$$

In the expression above, the second and third terms on the right-hand side respectively define q as the response to the optimal forcing f and a as the solution of the adjoint problem with forcing q. The last term ensures that f is an eigenfunction of $\mathscr{R}^\dagger \mathscr{R}$ with gain σ^2.

The gradient of the gain σ^2 with respect to base-flow modifications is derived by considering variations of the Lagrangian $\mathscr{K}$. Imposing the stationarity of the Lagrangian with respect to the adjoint variables yields the state equations, while the stationarity of the Lagrangian with respect to the state variables yields the equations to be satisfied by the adjoint variables. Since the operator $\mathscr{R}^\dagger \mathscr{R}$ is Hermitian, and thus self-adjoint, these equations are exactly the 'direct' equations if the adjoint variables are chosen so that $\{q^\dagger, a^\dagger, f^\dagger\} = \{a, q, f\}$ and if $(f^\dagger, f) = 1$. Therefore, the adjoint variables do not need to be computed since they are directly known from the state variables. The derivative of the Lagrangian with respect to the control variable gives the sensitivity function

$$\nabla_U \sigma^2 = 2\sigma^2 \text{Re}\{(\nabla f)u^* - (\nabla u^H)f\}. \tag{2.11}$$

In expanded format, this gradient is

$$\nabla_U \sigma^2 = 2\sigma^2 \text{Re}(u^* \partial_x f + v^* \partial_x f + w^* \partial_z f - f \partial_x u^* - g \partial_x v^* - h \partial_x w^*), \tag{2.12}$$

$$\nabla_V \sigma^2 = 2\sigma^2 \text{Re}(u^* \partial_x g + v^* \partial_y g + w^* \partial_z g - f \partial_y u^* - g \partial_y v^* - h \partial_y w^*), \tag{2.13}$$

$$\nabla_W \sigma^2 = 2\sigma^2 \text{Re}(u^* \partial_x h + v^* \partial_y h + w^* \partial_z h - f \partial_z u^* - g \partial_z v^* - h \partial_z w^*). \tag{2.14}$$

Here * indicates the complex conjugate of a scalar quantity. We recall that the optimal forcing is normalized so that $(\boldsymbol{f}, \boldsymbol{f}) = 1$ and the optimal response satisfies $(\boldsymbol{u}, \boldsymbol{u}) = \sigma^2$.

We note that the analysis presented here can be equivalently performed in the time domain. An outline of the derivation of the gradient of the norm of the evolution operator with respect to base-flow modifications is reported in the Appendix.

The sensitivity as given in (2.11) assumes arbitrary variations of the base flow. Such information is of interest because it gives the base-flow modifications leading to the largest variation of the energy gain. In other words it gives an upper bound on the energy variation that can be achieved by any base-flow modification. Yet, such variations should be interpreted with caution since they do not satisfy the Navier–Stokes equations. To gain further physical insight, it may be useful to enforce additional constraints on the type of variations allowed.

2.3. *Sensitivity to divergence-free base-flow modifications*

We focus here on the derivation of a divergence-free sensitivity field, denoted by $\overline{\boldsymbol{\nabla}_U \sigma^2}$, such that for any divergence-free base-flow variation $\delta \boldsymbol{U}$ the following equality holds:

$$\delta \sigma^2 = (\overline{\boldsymbol{\nabla}_U \sigma^2}, \delta \boldsymbol{U}) = (\boldsymbol{\nabla}_U \sigma^2, \delta \boldsymbol{U}). \tag{2.15}$$

The divergence-free sensitivity vector field can be written as the derivative of the scalar ψ: $\overline{\boldsymbol{\nabla}_U \sigma^2} = \partial_y \psi$, $\overline{\boldsymbol{\nabla}_V \sigma^2} = -\partial_x \psi$. It is straightforward to show that the function ψ satisfies

$$-\boldsymbol{\Delta} \psi = \partial_x (\boldsymbol{\nabla}_V \sigma^2) - \partial_y (\boldsymbol{\nabla}_U \sigma^2), \tag{2.16}$$

with $\boldsymbol{\nabla} \psi \cdot \boldsymbol{n} = n_y \boldsymbol{\nabla}_U \sigma^2 - n_x \boldsymbol{\nabla}_V \sigma^2$ imposed on all boundaries of the computational domain except on the lower boundary (see figure 5) where a symmetry boundary condition $\psi = 0$ is applied. Note that the definition of this sensitivity field is only of interest in a non-parallel context, since the divergence-free constraint is automatically satisfied in the parallel framework.

2.4. *Sensitivity to steady forcing and blowing/suction*

We focus here on the derivation of a sensitivity field for base-flow deviations satisfying the Navier–Stokes equations. They are produced either by introducing a two-dimensional forcing $\boldsymbol{F}$ in the base-flow momentum equations or by a non-homogeneous boundary condition at the wall, $\boldsymbol{U}_w$. Marquet *et al.* (2008) investigated the same problem for globally unstable flows. The sensitivity of the singular value is determined here in a similar way by first solving the following adjoint base-flow equations:

$$-(\boldsymbol{U} \cdot \boldsymbol{\nabla})\boldsymbol{U}^\dagger - (\boldsymbol{U}^\dagger \cdot \boldsymbol{\nabla})\boldsymbol{U}^\dagger = -\boldsymbol{\nabla} P^\dagger + Re^{-1}\nabla^2 \boldsymbol{U}^\dagger + \boldsymbol{\nabla}_U \sigma^2, \tag{2.17}$$

$$\boldsymbol{\nabla} \cdot \boldsymbol{U}^\dagger = 0, \tag{2.18}$$

where $(\boldsymbol{U}^\dagger, P^\dagger)$ are the adjoint base-flow fields whose boundary conditions are detailed in Marquet *et al.* (2008). The sensitivity to steady forcing is then determined by

$$\boldsymbol{\nabla}_F \sigma^2 = \boldsymbol{U}^\dagger, \tag{2.19}$$

while the sensitivity to wall blowing/suction is

$$\boldsymbol{\nabla}_{U_w} \sigma^2 = -P^\dagger \boldsymbol{n} + \frac{1}{Re}(\boldsymbol{\nabla} \boldsymbol{U}^\dagger) \cdot \boldsymbol{n}, \tag{2.20}$$

where $\boldsymbol{n}$ is a vector normal to the wall and pointing in the outward direction.

2.5. *Sensitivity and non-normality of the linearized Navier–Stokes operator for wall-bounded shear flows*

All terms involved in the gradient (2.11) are equal to the product of a component of the optimal forcing (f, g or h) with a component of the optimal response (u, v or w). Following Chomaz (2005) and Marquet *et al.* (2009), it is observed that the non-normality of the linearized Navier–Stokes operator (here the resolvent operator $\mathscr{R}$) makes the optimal forcing and optimal response orthogonal. Two types of non-normalities can be distinguished: the component-wise non-normality, which concentrates the optimal forcing and response on different components, and the streamwise non-normality, which separates the spatial supports of the structures, upstream for the optimal forcing and downstream for the optimal response. As shown by Monokrousos *et al.* (2010), the LU instability is characterized by an optimal forcing concentrated on the cross-stream g and spanwise h components while the optimal response is only on the streamwise component u. Inspection of the streamwise component of the sensitivity (2.12) immediately indicates that the LU perturbation is only weakly sensitive to streamwise base-flow modifications. This result is in agreement with the observations in Cathalifaud & Luchini (2000) and Zuccher, Luchini & Bottaro (2004) and can be deduced *a priori*. Streaks are ubiquitous in shear flows. On the other hand, the sensitivity should be much stronger for TS waves, since the streamwise and cross-stream components of both the optimal forcing and response structures have large magnitudes (e.g. Monokrousos *et al.* 2010). In addition, owing to the convective-type non-normality, the optimal forcing is located upstream while the optimal response is downstream. This means that the gradient is non-zero only in the region where the optimal forcing and response overlap. Hence, the stronger the convective non-normality, the weaker the gradient. This mechanism should act both on the LU instability and the TS instability, rendering the picture quite complex in open flows. For this reason, we first (§ 3) analyse the gradients in a parallel approach where we can focus on the effect of the component-type non-normality on the gradients of the LU and TS instabilities. Then in § 4, we consider a spatially developing boundary layer where both the component-wise non-normality and the convective non-normality are present.

It is worth mentioning that the gradient provided in (2.11) is formally identical to the sensitivity of an eigenvalue of the linearized Navier–Stokes problem to a modification of the base flow given in Marquet *et al.* (2008), once the adjoint and direct modes are replaced by the optimal forcing and response.

2.6. *Numerical method*

The equations defining the forced problem for a parallel base flow are discretized using Chebyshev collocation method in the y-direction (Weideman & Reddy 2000). For most of the computations presented we used $n_y = 121$, with n_y the number of collocations points. Tests were performed with $n_y = 201$ to validate the accuracy of the results. Homogeneous boundary conditions are applied to the forcing and velocity, $\hat{\boldsymbol{f}}$ and $\hat{\boldsymbol{u}}$, at the wall ($y = 0$) and in the free stream ($y = 30\delta^*$, where δ^* is the boundary layer displacement thickness).

The results for a spatially evolving boundary layer discussed in § 4 are obtained by a finite element approach. The spatial derivatives are discretized with Taylor–Hood finite elements ($P2$ elements for the velocity field and $P1$ elements for the pressure). The mesh consists of 3.82×10^6 triangles and their size in the boundary layer region
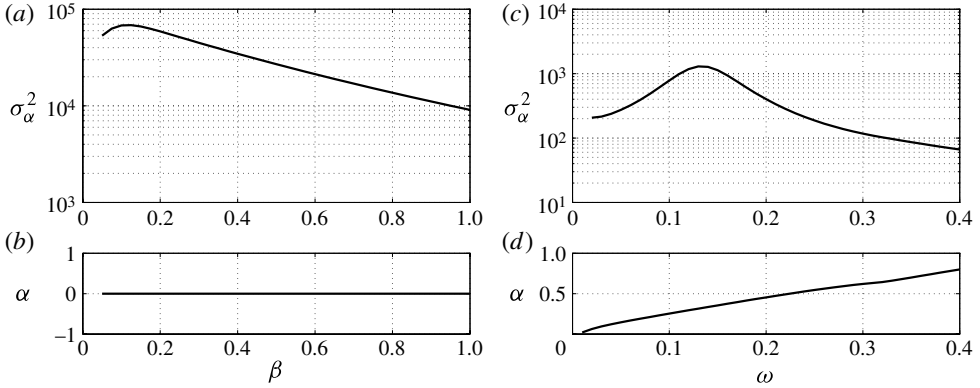
FIGURE 1. (*a*) Maximum optimal response σ_α^2 versus the spanwise wavenumber β for forcing frequency $\omega = 0$, Blasius flow at $Re_{\delta*} = 400$. (*b*) The streamwise wavenumber α pertaining to the largest response for each value of β and $\omega = 0$. (*c*) Maximum optimal response σ_α^2 versus forcing frequency ω for two-dimensional forcing $\beta = 0$. (*d*) The wavenumber α pertaining to the largest response.

$(-0.5 \leqslant x \leqslant 1.25, -1/600 \leqslant y \leqslant 0.02)$ is $\Delta x = 1/6000$ except near the ellipitcal leading edge where $\Delta x = 1/108\,000$. This results in a maximal number of degrees of freedom equal to ~ 25 million. The base flow is obtained with the Newton method while the computation of the largest singular values takes advantage of Krylov methods (ARPACK package, see www.caam.rice.edu/software/ARPACK/). All matrix inversions are performed by a direct LU multifrontal solver (MUMPS package, see http://graal.ens-lyon.fr/MUMPS/).

3. Sensitivity of perturbations in a parallel boundary layer flow

The zero-pressure-gradient boundary layer flow is a spatially developing flow. However, owing to the weak downstream growth of the shear layer, its stability has been traditionally studied under the assumption of parallel flow. Studying the evolution of perturbations of a parallel base flow $U = U(y)$ is a computationally easier task that enables a complete parameter study to be conducted. Despite the approximation made, such analysis has been shown to provide useful indications for the fully non-parallel flow. Thus the sensitivity results are first detailed for the parallel boundary layer with focus on the component-wise non-normality. The spatially evolving flow is examined in the next section in the global framework, where focus is on the analysis of the streamwise non-normality.

We present results for a parallel Blasius boundary layer at Reynolds number lower than $Re_{\delta*} = 500$. Above this critical value the Blasius velocity profile is locally convectively unstable and the analysis detailed in the previous section cannot be performed. The reader should then refer to the formalism developed by Bottaro *et al.* (2003). The Reynolds number is defined here using the free-stream velocity U_∞, the boundary layer displacement thickness δ^* and the kinematic viscosity ν, $Re_{\delta*} = U_\infty \delta^* / \nu$.

The maximum over all streamwise wavenumbers α of the energy amplification, $\sigma_\alpha^2(\omega, \beta; Re_{\delta*}) = \max_\alpha \sigma^2(\omega, \alpha, \beta; Re_{\delta*})$, is reported in figure 1 for the Reynolds number $Re_{\delta*} = 400$. The analysis focuses on the LU and TS mechanisms separately and considers an optimization over the streamwise scale of the disturbance to

more easily compare with the global analysis presented next. The results for time-independent modes (LU) are displayed in figure 1(a,b), whereas two-dimensional modes are illustrated in figure 1(c,d). Similar results can be found in Corbett & Bottaro (2000) and Schmid & Henningson (2001) for the analysis of the optimal transient growth. The largest amplification for LU is obtained for spanwise wavenumber of the forcing $\beta = 0.12$, while the TS waves are more receptive to forcing at frequency $\omega = 0.13$ for the Reynolds number considered. The real values of α associated with the maximum responses shown in figure 1(a,c) are displayed in figure 1(b,d). Not surprisingly, the steady LU mechanism is associated with streamwise-independent perturbations while the streamwise wavenumber of the optimal TS-waves increases with the forcing frequency.

The profiles of the optimal forcing and response for the two growth mechanisms under investigation are shown in figure 2. The largest amplification is due to the LU mechanism and indeed the optimal forcing displayed in figure 2(a) has the form of streamwise-independent vortices and induces an optimal flow response organized as streamwise velocity streaks, seen in figure 2(b). For the TS-modes the optimal excitation is mainly of streamwise momentum and located close to the critical layer, where the base-flow velocity is equal to the phase speed of the TS wave. The flow response has the typical shape of these modes (see figures 2c and 2d).

The sensitivity of the optimal harmonic excitation to variations of the base flow $\nabla_U \sigma^2(y; \omega, \alpha, \beta)$, i.e. the gradient of the largest singular value of the resolvent operator with respect to base-flow modifications, is shown in figure 3. As a measure of the sensitivity, function of the wall-normal coordinate y, we choose the cross-stream maximum and normalize it with the corresponding energy gain, i.e. $\max_y |\sigma^{-2} \nabla_U \sigma^2(y)|$. This quantity is displayed in figure 3(a,b) for streaks and TS-waves and the wavenumber α maximizing the amplification σ_α^2 shown in figure 1. The results indicate that the sensitivity is stronger for the case of time-dependent disturbances and exhibit a peak where the flow response is also largest. The sensitivity is much weaker for time-independent streaky forcing. The variation of the sensitivity with the Reynolds number is explored in figure 3(c). Here the sensitivity $\nabla_U \sigma^2$ is reported to document also the absolute values of the gradient. The sensitivity for streaky disturbances, depicted by filled symbols, is only slightly increasing with $Re_{\delta*}$, while the energy gain σ^2 scales as $Re_{\delta*}^2$ (Schmid & Henningson 2001). The sensitivity of the TS disturbances, initially weaker, becomes clearly dominant, about three orders of magnitude larger, on approaching the critical Reynolds number (branch I). The data suggest that at higher Reynolds numbers weak modifications of the base flow can have a significant impact on the excitation of TS-like disturbances while streamwise streaks are more difficult to alter. In a parallel flow, small defects can easily make the flow linearly unstable as shown by Bottaro *et al.* (2003) for Couette flow.

The wall-normal profiles of the sensitivity to base-flow modifications $\nabla_U \sigma^2(y)$ for the two dominant instabilities in Blasius flow are reported in figure 4. Results are shown for $\omega = 0$, $\beta = 0.1$ and $\omega = 0.13$, $\beta = 0$. Further, the shape of the sensitivity profiles does not show significant variation with the Reynolds number; the profiles displayed correspond to modifications that would induce an increase of the flow response. To affect the LU mechanism, base-flow modifications are required throughout the flow, see figure 4(a). Reduction of the mean velocity at the boundary layer edge and increase in the free stream both contribute to an increase of the boundary layer thickness, as in the case of adverse pressure gradient which is known to promote streak amplification. In figure 4(b), it is seen that a decrease of the base flow velocity at the height of the critical layer, followed by an increase at the
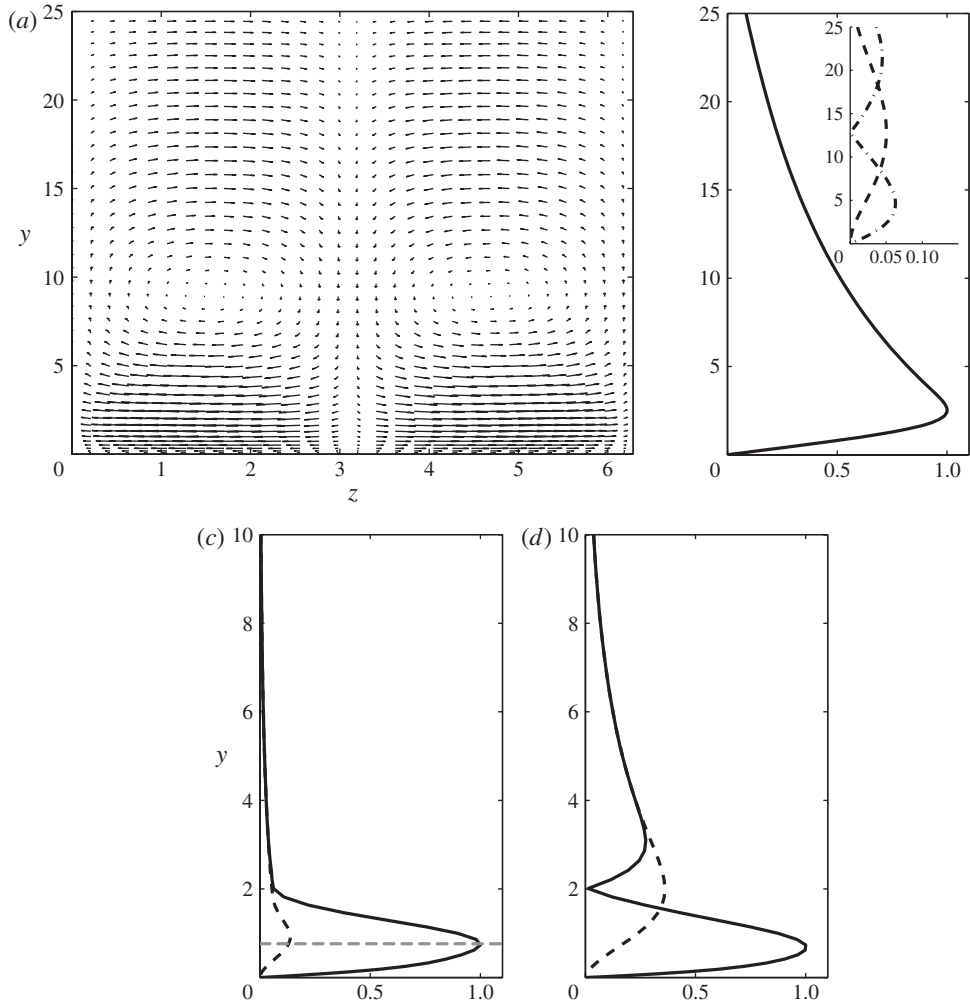
FIGURE 2. (a) Optimal forcing for $\omega = 0$, $\beta = 0.1$ and $Re_{\delta*} = 400$ in the cross-stream y–z plane and (b) corresponding wall-normal profile of optimal response. (c) Wall-normal profile of the optimal forcing for $\omega = 0.13$ and $\beta = 0$ with optimal response in (d).The dashed–dotted line in (c) indicates the location of the critical layer. Solid line: streamwise velocity u; dashed line: wall-normal velocity v; dashed-dotted line: spanwise velocity w, when $\beta \neq 0$.

sides, would induce a stronger time-periodic response in the flow. Such a base-flow modification may be induced by a small object placed at the distance from the wall where the local velocity is the phase speed of the least-stable wave. The results are in qualitative agreement with the findings in Pralits *et al.* (2000) who considered sensitivity of TS waves to an external disturbance source within the framework of the parabolized stability equations. Note, finally, that the region of highest sensitivity is located closer to the wall for time-dependent forcing than for steady excitations. This strongly suggests that the amplification of streaks is much less sensitive to base-flow modifications that can be created from the wall.
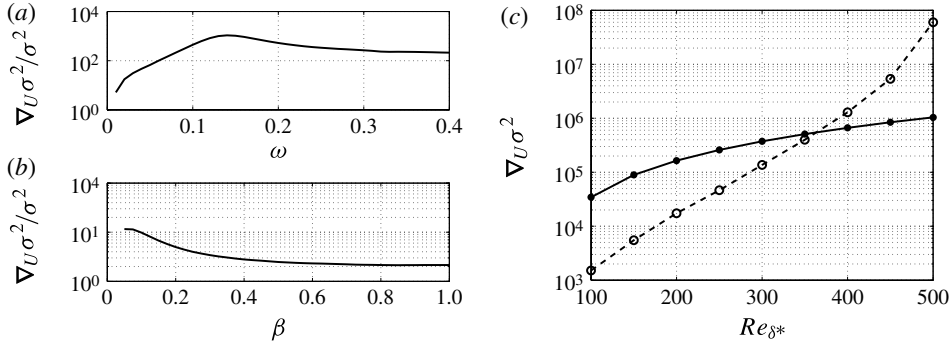
FIGURE 3. (*a,b*) Normalized sensitivity $\sigma^{-2}\nabla_U\sigma^2$ of the optimal forcing with respect to base-flow modification for Blasius flow at $Re_{\delta*} = 400$: (*a*) wall-normal maximum of the sensitivity versus ω for TS-instabilities, $\beta = 0$; (*b*) wall-normal maximum of the sensitivity versus β for LU-instabilities, $\omega = 0$. (*c*) Reynolds-number behaviour of the sensitivity for forcing with $\omega = 0.13$, $\beta = 0$ (open symbols), and $\omega = 0$, $\beta = 0.1$ (filled symbols).
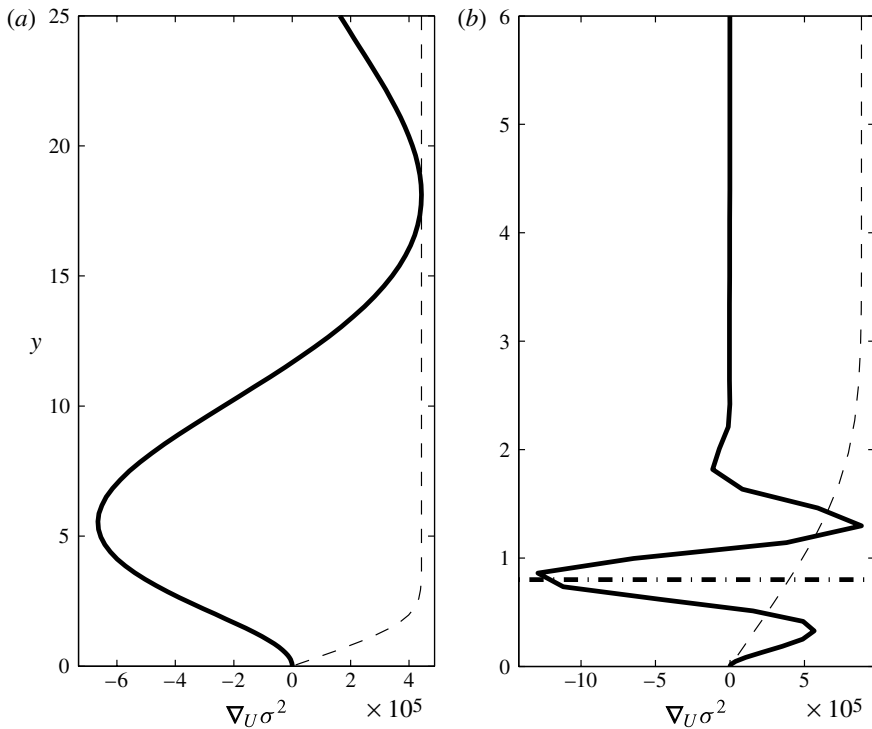
FIGURE 4. Wall-normal profile of the gradient of the optimal response to base-flow modification $\nabla_U\sigma^2$ for parallel Blasius flow, $Re_{\delta*} = 400$: (*a*) $\omega = 0$ and $\beta = 0.1$; (*b*) $\omega = 0.13$, $\beta = 0$ and $\alpha = 0.315$. The thin dashed line depicts the Blasius profile, while the dashed–dotted in line in (*b*) indicates the location of the critical layer.

The weak sensitivity of streaks to base-flow modifications demonstrated above can also be inferred by considering the linearized stability equations for parallel base flow and streamwise independent disturbances ($\alpha = 0$). In this limit the Orr–Sommerfeld

equation becomes independent of the base flow. The latter appears only on the right-hand side of the Squire equation (in particular its wall-normal derivative). This implies that a small variation of the base flow can only have a small effect on the eigenfunctions of the Squire problem. The non-modal behaviour can be explained by the forcing of Squire modes from eigenfuncions of the Orr–Sommerfeld equation and therefore the effect of any variation of the base flow can be expected to be small. In addition, the most involved modes are those least stable, i.e. those with lower variations in the wall-normal distribution, which are less affected by localized modifications.

Streak non-modal amplification in boundary layers is triggered by disturbances in the free stream in an unbounded domain. It is possible to show how streaks can be induced by free-stream modes associated with the continuous spectrum of the stability equations (Grosch & Salwen 1978; Brandt, Schlatter & Henningson 2004; Zaki & Durbin 2005). These are modes oscillating periodically in the free stream and decaying to zero inside the shear layer. The continuous spectrum is formed at infinity and therefore its eigenvalues cannot be affected by base-flow modification that can be created in practice by actuation at the wall. Although the eigenfunctions are dependent on the specific base-flow profile, their decay rate is determined in the free stream and therefore one cannot diminish the modes' capability to act as forcing term for streamwise-velocity perturbation. Note however that optimal disturbances in spatially evolving boundary layers over finite-length domains are located closer to the shear layer as discussed in § 4 and in Monokrousos *et al.* (2010).

4. Sensitivity of perturbations in a spatially evolving boundary layer

In this section, we investigate the stability and sensitivity of a spatially evolving boundary layer. Unlike the previous global stability analysis dedicated to the development of perturbations in boundary layers, we consider a flow configuration where the leading edge of the flat plate is included in the computational domain. Single frequency–wavenumber vortical modes impinging on an elliptic leading edge have been recently analysed by Schrader *et al.* (2010). The computational domain is shown in figure 5: the flat plate is located at $y = 0$ and extends from $x = 0$ to 1.25 with an elliptical leading edge of aspect ratio 3 as depicted in the inset of the figure. The inlet boundary is located upstream of the leading edge at $x = -0.5$ whereas the outflow boundary is at the end of the flat plate where $x = 1.25$. An upper boundary is placed at $y = 0.25$ and a lower boundary connects the inlet to the leading edge. All lengths have been made non-dimensional with a reference length l shorter than the flat-plate length. This choice will be explained later.

To compute the base flow a uniform velocity profile, $u = u_\infty = 1, v = 0$, is imposed at the inlet, the free-stream velocity u_∞ being used as the reference velocity. Symmetric boundary conditions are applied on the upper and lower boundaries, no-slip boundary conditions are applied on the wall and an outflow boundary condition, commonly used in finite-element computation, is enforced on the outlet boundary: $(p - (1/Re)\partial_x u = 0, \partial_x v = 0)$. The Reynolds number based on the reference length and velocity is fixed to $Re = 6 \times 10^5$. Figure 6 displays the characteristics of the base flow. The pressure coefficient shown in figure 6(*a*) exhibits strong variations around the leading edge. On the flat plate ($x > 0$) the presence of the leading edge induces a favourable pressure gradient until $x \approx 0.1$. Further downstream we observe a slight adverse pressure gradient indicating that the boundary layer is not strictly a zero-pressure-gradient boundary layer. The local displacement thickness δ^* is depicted
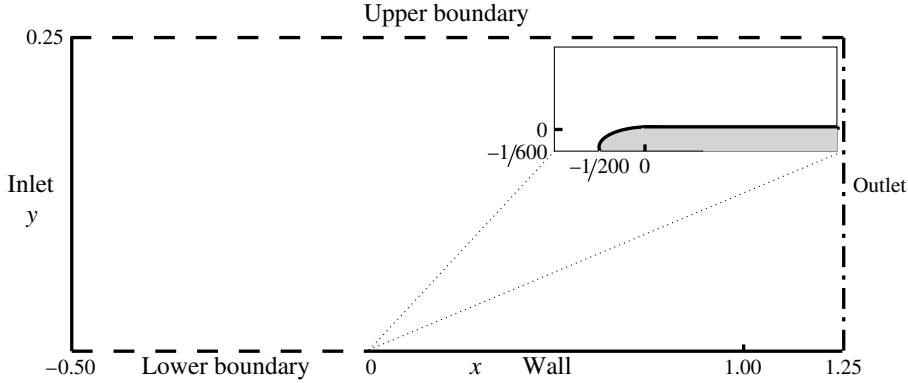
FIGURE 5. Computational domain used for the spatially developing boundary layer.
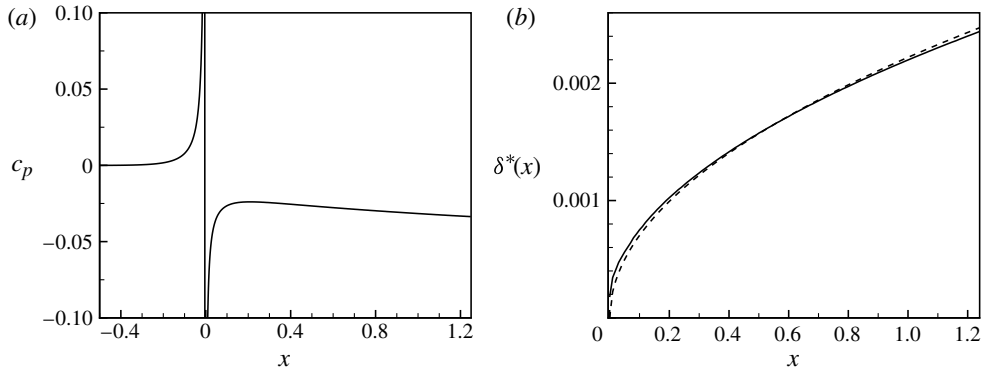

FIGURE 6. Characteristics of the base-flow computed at $Re = 6 \times 10^5$. (a) Pressure coefficient and (b) displacement thickness as a function of the streamwise coordinate x. For comparison, the dashed line indicates the Blasius boundary layer solution.

in figure 6(b) and is compared to the analytic expression $1.72Re^{-1/2}\sqrt{x}$ obtained for the asymptotic Blasius similarity solution. At the beginning of the flat plate the displacement thickness is equal to 1.7×10^{-4} which corresponds to a Reynolds number based on the displacement thickness of $Re_{\delta*} = 106$. At $x = 1$, δ^* is equal to 1317 and reaches 1465 at the outlet $x = 1.25$. Despite the slight adverse pressure gradient observed on the flat plate, the development of the boundary layer is very close to the Blasius solution. In the following the displacement thickness at the station $x = 1$ will be denoted $\delta = \delta^*(x = 1)$ for convenience and the frequency $F = 10^6 \times \omega/Re$ will be used to present the results.

4.1. *Optimal forcing and response*

The stability of the boundary layer is not investigated in the whole computational domain but in a restricted domain extending up to $x = l = 1$, the reference length. Thus we define the optimal energy gain σ^2 as the ratio of the energy of the optimal response in the restricted domain $x \leqslant 1$ to the energy of the optimal forcing in the whole domain. This choice ensures that the following results are free from any numerical effects due to the outflow boundary condition. Indeed numerical tests have been carried out to check that the base-flow pressure coefficient, the spatial distribution
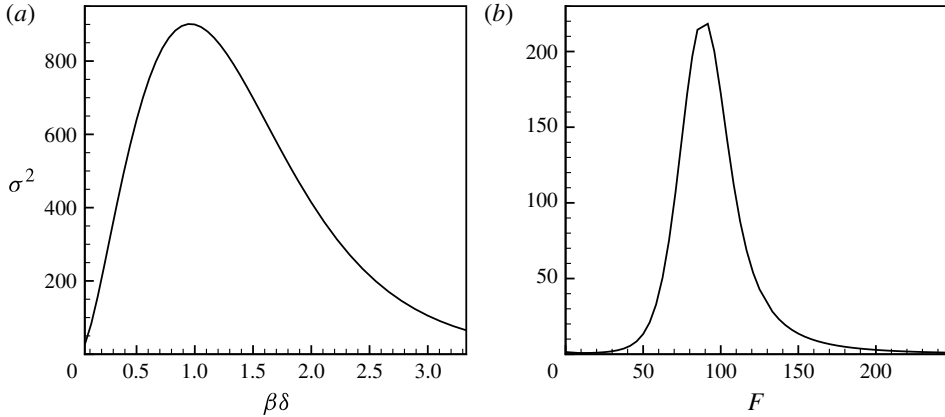
FIGURE 7. Spatially developing boundary layer: optimal gains σ^2 for (*a*) the steady three-dimensional (LU) perturbations ($\beta \neq 0$) and (*b*) the harmonic two-dimensional (TS) perturbations ($F \neq 0$).

of the optimal forcing and response, as well as the optimal gain, vary by less than 1 % when limiting the domain to $x = 1.125$.

The optimal gains σ^2 have been computed for two types of perturbations: steady three-dimensional perturbations ($F = 0$, $\beta \neq 0$) and harmonic two-dimensional perturbations ($F \neq 0$, $\beta = 0$). Oblique perturbations ($F \neq 0$, $\beta \neq 0$) have not been investigated in the present study. Figure 7(*a*,*b*) shows the optimal gains obtained for both types of perturbation, as a function of the spanwise wavenumber $\beta \delta$ and of the frequency F respectively. The largest amplification for steady three-dimensional perturbations $\sigma^2 \sim 900$ is obtained for the spanwise wavenumber $\beta \delta = 0.94$ while two-dimensional harmonic perturbations display a maximum gain of $\sigma^2 \sim 222$ for the frequency $F = 88$. In the present study the three-dimensional steady perturbations are thus more amplified than the two-dimensional harmonic perturbations. This is not a general feature and for larger Reynolds number we would expect different results. Indeed Åkervik *et al.* (2008) and Monokrousos *et al.* (2010) have given similar curves $\sigma^2(F)$ but for a boundary layer flow configuration where the leading edge was not included in the computational domain. In the latter study where the inlet and outlet Reynolds numbers were equal to $Re_{\delta*} = 1000$ and 1834 respectively, it was found that the two-dimensional harmonic perturbations were more amplified than the three-dimensional steady perturbations. Therefore we can expect that for larger Reynolds number the two-dimensional harmonic perturbations would have larger gains. Before turning to the description of the forcing and response structures, it is worth mentioning that these large gains correspond to a pseudo-resonance of the linearized Navier–Stokes operator: they cannot be explained solely by the presence of a particular eigenvalue in the spectrum of this operator near the forcing frequencies $F = 0$ or 88 as shown in Åkervik *et al.* (2008) and Alizard, Cherubini & Robinet (2009).

To describe the spatial structures of the optimal forcing and response we will use the energy density of the perturbation. For a scalar field f, the energy density is defined by $d_f(x) = \int_0^1 (|f|^2) \, dy$ while for a vector field $\boldsymbol{f} = (f, g, h)$ it is defined by $d_f(x) = \int_0^1 (|f|^2 + |g|^2 + |h|^2) \, dy$. Figure 8 shows the energy density of the optimal forcing and response as a function of the streamwise coordinate x. The case of three-dimensional steady perturbations is depicted in figure 8(*a*) for the wavenumber
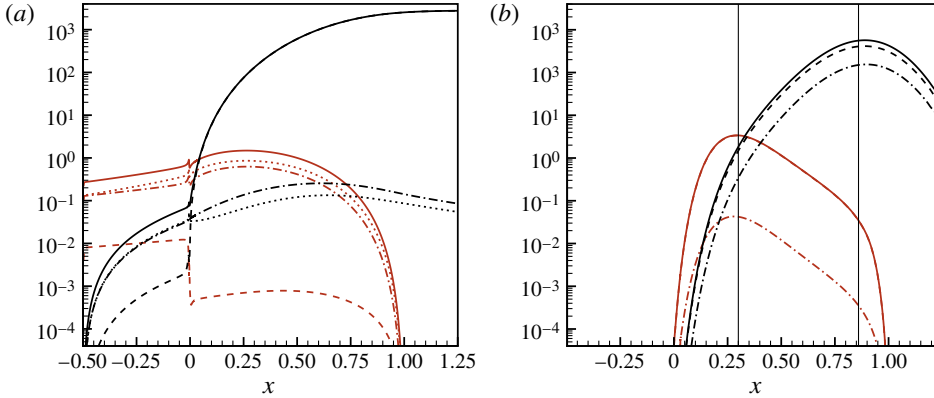
FIGURE 8. Density functions of (*a*) the three-dimensional steady (LU) optimal perturbation at $\beta\delta = 0.94$ and (*b*) the two-dimensional harmonic (TS) perturbation at $F = 100$ as a function of the streamwise coordinate. The red and black lines depict the optimal forcing and response respectively. For each case, the solid lines indicate the density energy while the dashed, dashed–dotted and dotted lines are used for the streamwise, cross-stream and spanwise components. The vertical lines in (*b*) delimit the convectively unstable region.

$\beta\delta = 0.94$ while the case of two-dimensional harmonic perturbations is shown in figure 8(*b*) for the frequency $F = 100$.

For the three-dimensional steady perturbation the spatial distribution of the optimal forcing and response associated with the dominant singular value is depicted in figure 9. For clarity the vertical coordinate has been non-dimensionalized by δ. The evolution of the local displacement thickness δ^* and boundary layer thickness $\delta_{0.99}$ is indicated in the figure by the dashed and solid lines respectively. The optimal forcing is represented in figure 9(*a*) by iso-contours of its spanwise component while the optimal response is shown in figure 9(*b*) by isocontours of the streamwise velocity. First we note that the structures are weakly varying in the streamwise direction, which relates to the $\alpha = 0$ perturbations described in §3. On the flat plate ($x > 0$) the optimal forcing is dominated by the cross-stream velocity components while the response is concentrated in the streamwise component. This is a footprint of the component-type non-normality of the linearized Navier–Stokes operator which can be explained in the present case by the LU instability mechanism: streamwise vortical structures induce streamwise velocity streaks. In addition, the optimal forcing, strongest near $x = 0.25$, tends to be located on the upstream part of the flat-plate while the response is largest downstream of the flat plate. This stems from the convective-type non-normality, separating the spatial supports of the optimal forcing and response. Interestingly, the optimal forcing remains at significant amplitudes even upstream of the flat plate ($x < 0$). In this region the optimal forcing and response are dominated by their cross-stream components, indicating that the LU instability mechanism is not yet at play. Instead, the optimal forcing creates streamwise vorticity by stretching and tilting upstream disturbances through the shear induced by the leading edge (see also Schrader *et al.* 2010). This vorticity would trigger streaks only when impinging on the plate.

For the two-dimensional harmonic waves the spatial distribution of the optimal forcing and response pertaining the dominant singular value are depicted in figure 10 for $F = 100$. Here we focus our attention on this frequency even if it is not exactly
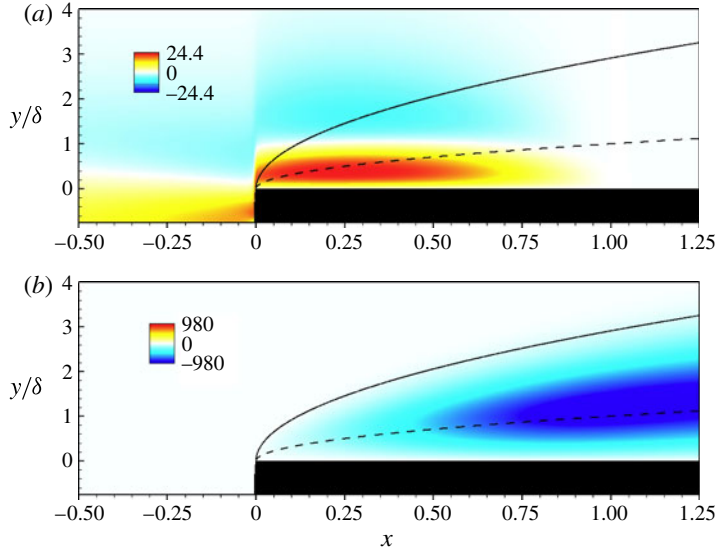
FIGURE 9. Optimal three-dimensional steady (LU) perturbation for $\beta\delta = 0.94$. (a) Spanwise component h of optimal forcing. (b) Stream-wise component u of optimal response.
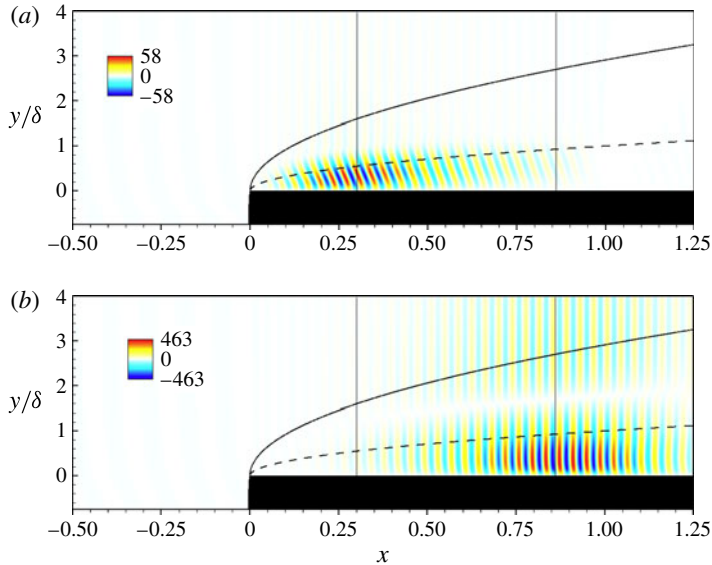

FIGURE 10. Optimal two-dimensional harmonic (TS) perturbation for $F = 100$. (a) Stream-wise component f of optimal forcing. (b) Stream-wise component u of optimal response. The vertical thin solid lines denote the location of branch I and branch II, as defined by local stability theory.

the optimal frequency because branches I and II, as determined by local stability theory, are both within the optimization domain. We note that the disturbance consists of a series of waves of characteristic streamwise scale related to the wavenumber α considered in the analysis of a parallel boundary layer (§ 3). The flow response is

clearly localized downstream of the flat plate and reaches a maximum around $x = 0.90$. This station is very close to the location of branch II, $x = 0.88$ for $F = 100$, where the nature of the local stability changes from convectively unstable to stable. On the other hand the optimal forcing is localized upstream and reaches a maximum around $x = 0.25$, slightly upstream of the location of branch I, $x = 0.29$ for $F = 100$, where the local stability of the flow changes from stable to convectively unstable. This shows that the strong convective non-normality of the underlying global operator is here closely related to the local stability of the flow. We also emphasise that the optimal forcing drops off very quickly upstream of branch I, and therefore harmonic forcing located upstream of the flat plate is very inefficient at triggering TS waves. Similarly, the optimal response weakens downstream of branch II. These features markedly differ from those described for the LU instability. Finally the footprint of the component-type non-normality is seen on the structure of the optimal forcing, which is dominated by its streamwise component, while the optimal response is equally distributed on its streamwise and cross-stream components. The streamwise forcing is dominant because the forcing is leaning against the shear of the base flow. Thus the well-known Orr mechanism is also at play to efficiently initiate the TS instability as explained in Åkervik *et al.* (2008).

4.2. *Sensitivity to base-flow variations*

Before presenting the sensitivity field in the global framework, we note that instead of depicting the field $\nabla_U \sigma^2$, we have chosen to show the quantity $\delta^2 \sigma^{-2} \nabla_U \sigma^2$. If we consider a base-flow variation of small amplitude ϵ, localized on a area δ^2 around the location (x_0, y_0), (2.8) shows that the variation of the singular value is approximated by $\delta \sigma^2 = \epsilon \delta^2 \nabla_U \sigma^2 (x_0, y_0)$. The chosen quantity is thus the rate of variation of the energetic gain divided by the amplitude of a base-flow variation localized on a surface δ^2.

The sensitivity to base-flow variation of the TS perturbation previously described is first investigated. Figure 11 displays the density of sensitivity fields as a function of the streamwise coordinate x. First we focus on the sensitivity to generic base-flow variations which is depicted in figure 11(*a*). This sensitivity field is largest in the region of the flow located between branch I and branch II, indicating that TS perturbations are only sensitive to base-flow variations in the convectively unstable region. This result is reminiscent of the streamwise distribution of the optimal forcings and responses shown in figures 8(*b*). Roughly speaking the sensitivity is defined as the product of the optimal forcing and response so that it can only be strong in the region where these overlap. For TS perturbations, the sensitive region corresponds to the convectively unstable region. Moreover we observe that TS perturbations are slightly more sensitive to cross-steam variations than to streamwise variations. This result should be interpreted with caution. Indeed although generic base-flow variations are allowed they may be not physical since they do not satisfy the governing equations.

To gain more physical insight, we therefore focus our attention on divergence-free base-flow variations and compute an appropriate sensitivity field as explained in § 2.3. Results are displayed in figure 11(*b*). We see that the sensitivity to cross-stream variations has vanished while the sensitivity to streamwise variations is almost unaltered. This result is interesting in terms of flow control since only divergence-free base-flow variations may be produced. Consequently, even if the sensitivity to generic base flow variation is strong in the cross-stream direction, this cannot be exploited for flow control. Figure 12 depicts the streamwise component of the divergence-free sensitivity field. The spatial distribution is shown in figure 12(*a*) while a wall-normal
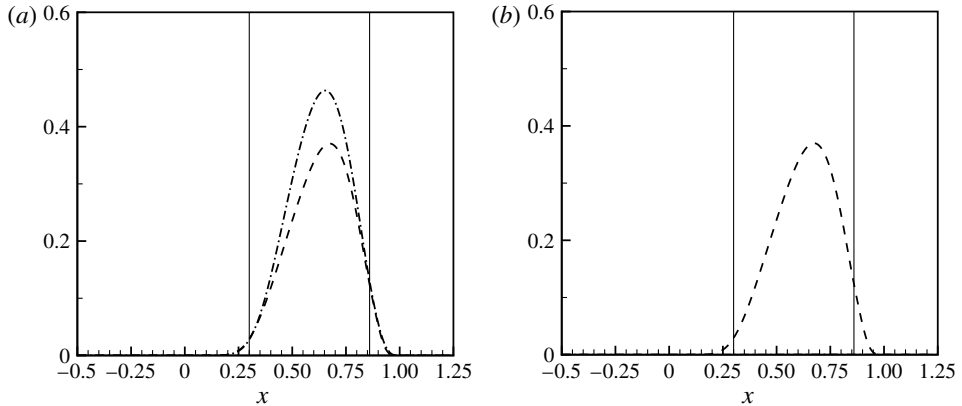
FIGURE 11. Sensitivity of the TS perturbation to (*a*) generic and (*b*) divergence-free base-flow variations. The dashed (dash-dotted) line depicts the density of the streamwise (cross-stream) component of the sensitivity fields (*a*) $\delta^2\sigma^{-2}\nabla_U\sigma^2$ and (*b*) $\delta^2\sigma^{-2}\overline{\nabla_U}\sigma^2$. $F = 100$.
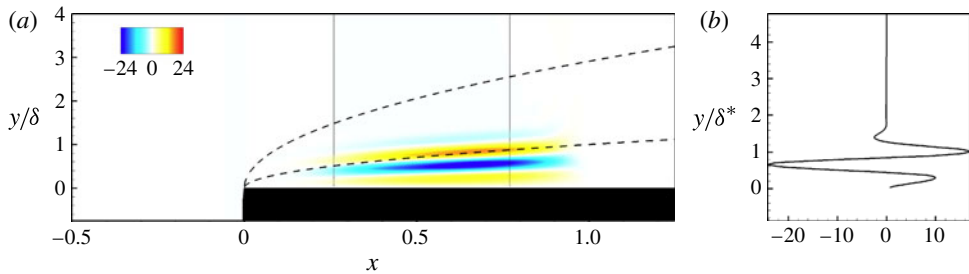

FIGURE 12. Sensitivity of TS perturbations to divergence-free base-flow variations. (*a*) Spatial distribution of the streamwise component of the field $\delta^2\sigma^{-2}\overline{\nabla_U}\sigma^2$. (*b*) Wall-normal profile of the sensitivity at the station $x = 0.7$. The *y* coordinate is here normalized with the local displacement thickness $\delta^*(x = 0.7)$. $F = 100$.

profile is represented in figure 12(*b*) for comparison with the parallel results shown in figure 4(*b*). This field is weakly varying in the streamwise direction but exhibits strong variations in the cross-stream direction. These variations are quite similar to those found in the parallel case. The sensitivity profile in figure 12(*b*) strongly resembles the wake defect that would be observed behind an object placed at $y = 0.6\delta^*$.

The sensitivity of the LU perturbation is presented in figures 13(*a*) and 13(*b*), where we display the density functions for generic and divergence-free base-flow variations. First we emphasise that LU perturbations are much less sensitive to base-flow variations than TS perturbations. For instance, the sensitivity of the LU instability to divergence-free variations is three orders of magnitude lower than the sensitivity of the TS instability, as for the parallel boundary layer. Secondly we observe that the cross-stream component is largely dominant when generic variations are considered but this is again no longer valid when allowing only divergence-free modifications. Therefore, in the following discussion we focus on the results displayed in figure 13(*b*). The LU sensitivity exhibits a very sharp peak on the leading edge of the flat plate, the amplitude being two orders of magnitude larger than everywhere else in the flow. As seen in the inset of figure 13(*b*) and in figure 14, the location of this
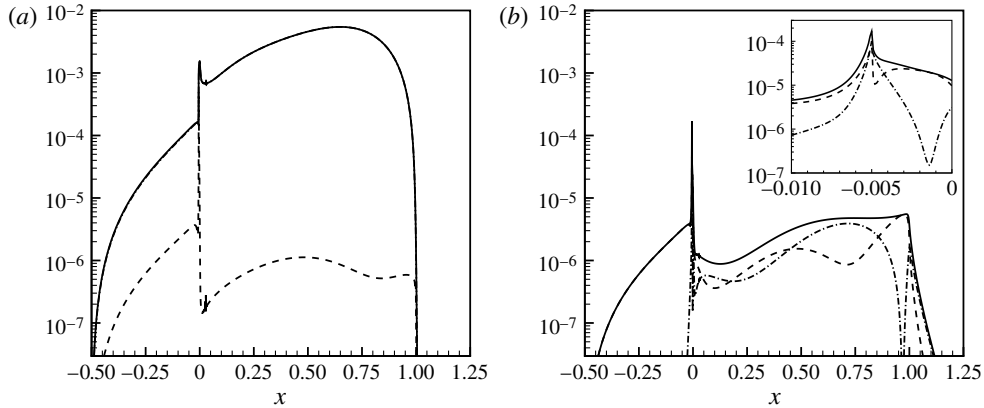
FIGURE 13. Sensitivity of LU perturbations to (*a*) generic and (*b*) divergence-free base-flow variations. The solid lines depict the density of the magnitude of the sensitivity while the dashed and dash-dotted lines indicate the streamwise and cross-stream components.
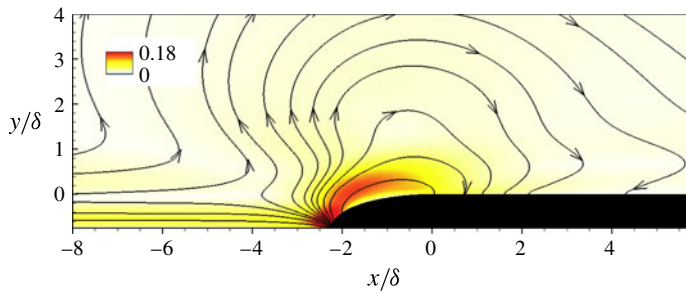

FIGURE 14. (Colour online available at journals.cambridge.org/flm) Sensitivity of LU perturbations to divergence-free base-flow variations. Spatial distribution of $\delta^2 \sigma^{-2} \overline{\nabla_U \sigma^2}$ close to the leading edge of the flat plate. The colours indicate the magnitude of the field and the lines show the directions. Note that here the x and y coordinates are normalized with the displacement thickness δ. $\beta\delta = 0.94$.

peak exactly corresponds to the position of the elliptic leading edge. Interestingly the sensitivities upstream of the flat plate ($x < 0$) and on the flat plate ($x > 0$) are of comparable magnitude. Upstream of the flat plate the LU perturbation is only sensitive to streamwise base-flow variations while modifications of the cross-stream component can affect the disturbance amplification above the flat plate.

As in §3, these findings may be explained by inspection of the expression of the gradient given in (2.11). Note that the sensitivity with respect to the spanwise component of the base flow W is zero for both TS and LU disturbances. This can be seen directly from the expression of the gradient for two-dimensional perturbations and for disturbances of zero frequency. In the latter case, the optimal forcing and response can be written in the form (f, g, ih) and (u, v, iw) and hence the gradient with respect to W is zero since it is given by the real part of a purely imaginary term (see (2.11)). In both cases, for symmetry reasons, positive and negative distortions should be equivalent since the flow is homogeneous in the spanwise direction. However, $\nabla_W \sigma^2$ should be considered for oblique waves when both F and β are non-zero.
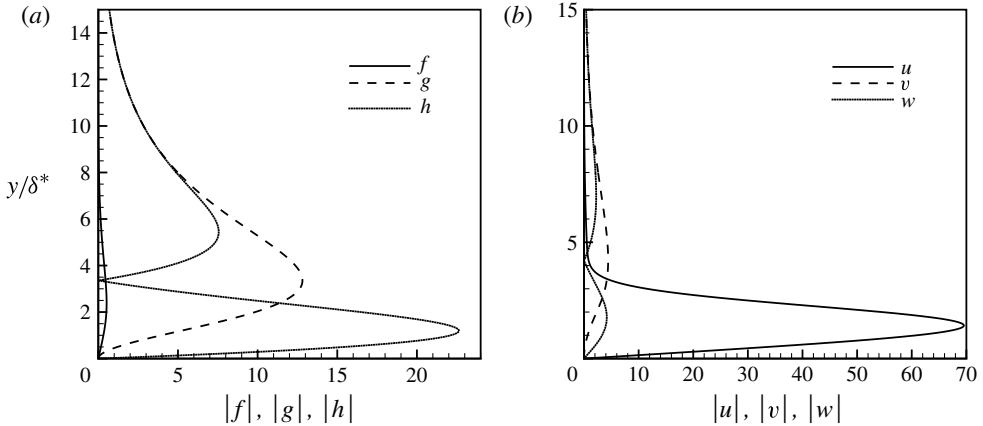
FIGURE 15. Wall-normal profiles of the optimal forcing (*a*) and response (*b*) extracted at the downstream position $Re_{\delta*} = 400$ for the LU perturbation $\beta\delta = 0.94$. The spanwise wavenumber non-dimensionalized by the local displacement thickness is equal to $\beta\delta^* = 0.283$. The solid, dashed, dashed–dotted lines refer to the streamwise, cross-stream and spanwise components. These figures may qualitatively be compared to the local results of figure 2(*a*,*b*).

4.3. *Comparison of local and global analysis*

In this section, we compare the results from the local and global analysis. For this, we have extracted from the global results the wall-normal profiles of the optimal forcing, optimal response, and gradient at the streamwise station corresponding to $Re_{\delta*} = 400$. The data for the LU case ($F = 0$, $\beta\delta = 0.94$), are represented in figure 15, while those for the TS case ($F = 100$, $\beta = 0$) are reported in figure 16. The spanwise wavenumber of the LU instability, non-dimensionalized with the local displacement thickness, is $\beta\delta^* = 0.283$, while the frequency of the TS instability is $\omega\delta^*/U_\infty = 0.133$. The results in figures 15 and 16 may therefore be compared to those of figure 2. It is seen that in the LU case the optimal forcing and response in the spatially evolving boundary layer are located closer to the wall than in the case of the parallel boundary layer. In the global approach, the perturbation evolution is monitored over a finite-length domain and although a forcing located further outside the boundary layer would certainly be more effective, it would also require longer distances to interact with the shear layer close to the wall. This would imply a larger growth but further downstream, outside our optimization domain. In a parallel flow, conversely, there is no limitation on the distance travelled by the disturbances before reaching the largest energy amplification. In the case of TS waves, the local and global results qualitatively agree. Similar trends may be observed for the sensitivity displayed in figure 17: while the profiles qualitatively agree with those for a parallel flow for the TS waves, the gradient is closer to the wall in the global approach. This result is directly related to the differences in the wall-normal location of the optimal forcing and response mentioned above.

4.4. *Towards flow control: sensitivity to steady forcing and blowing/suction*

As a first step towards feasible passive control of perturbations in boundary layers we investigate two different ways to produce base-flow modifications: a two-dimensional steady momentum forcing and blowing/suction on the plate.
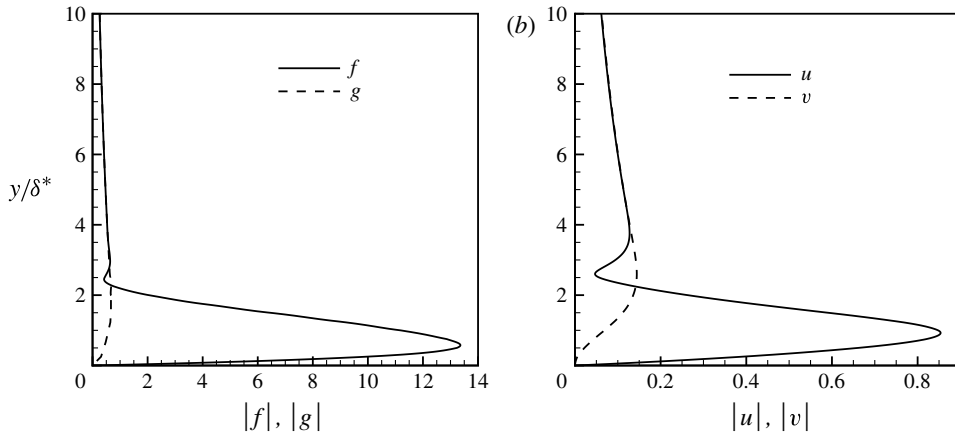
FIGURE 16. Same as figure 15 but for the TS perturbation $F = 100$. The frequency non-dimensionalized by the local displacement thickness is equal to $\omega\delta^*/U_\infty = 0.133$. These figures may qualitatively be compared to the local results of figure 2(c,d).
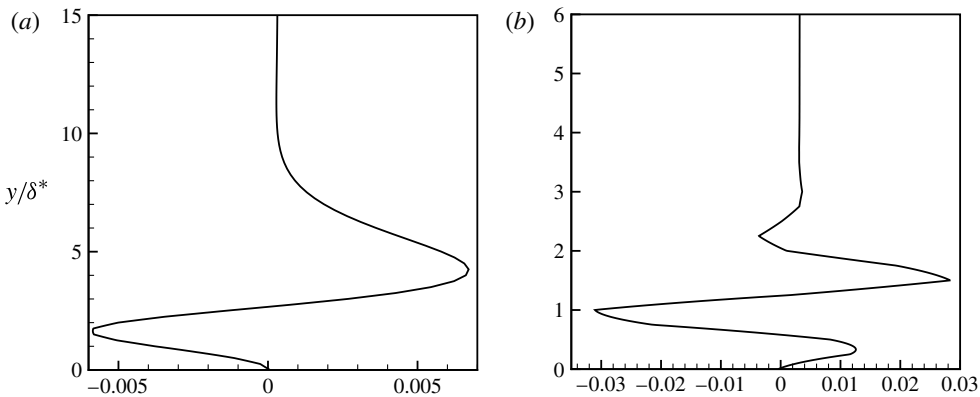

FIGURE 17. Wall-normal profiles of the streamwise component of the sensitivity $\sigma^{-2}\nabla_U\sigma^2$ for (a) the LU instability, (b) the TS instability shown in the previous figures. These figures may be qualitatively compared to the local results of figures 4(a,b).

The sensitivity fields to steady forcing introduced in §2.4 have been computed for the TS and LU perturbations and in both cases the streamwise component is dominant. Figure 18(a) thus displays the density of this component as a function of the streamwise coordinate. As noted previously, the TS perturbation is much more sensitive than the LU perturbation. In particular, the TS perturbation is mainly sensitive to forcing located between branch I and branch II while the LU perturbation is also sensitive to forcing located upstream of the flat plate. As opposed to the divergence-free sensitivity field, we do not observe any sharp peak around the leading edge in the case of LU perturbations. Figure 19 shows the spatial distribution of the streamwise component of the sensitivity for both LU and TS perturbations. To interpret these figures let us consider a force acting in the direction of the base flow and localized on a area δ^2 centred around $(x, y) = (0.7, 0.4)$. If the amplitude ϵ of this force is small, the energy of the TS perturbations is expected to decrease as
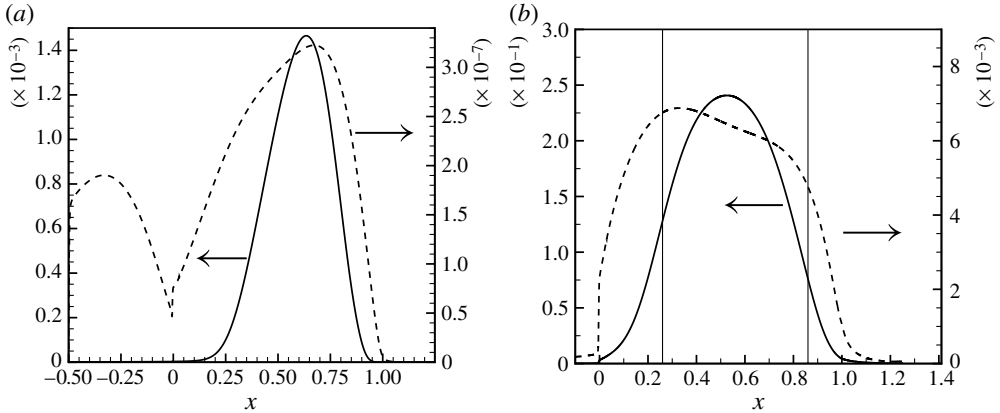
FIGURE 18. (*a*) Density of the streamwise component of the sensitivity to steady forcing $\delta^2\sigma^{-2}\mathbf{\nabla}_F\sigma^2$ and (*b*) sensitivity to wall-normal blowing/suction $\delta^2\sigma^{-2}\mathbf{\nabla}_{U_w}\sigma^2$ as a function of the streamwise coordinate. The solid and dashed lines depict the results for TS ($F = 100$) and LU ($\beta\delta = 0.94$) perturbations respectively. Note that the values on the left axis pertain to the sensitivity of the TS disturbance and the values on the right to the sensitivity of the LU disturbance, the latter being significantly smaller.
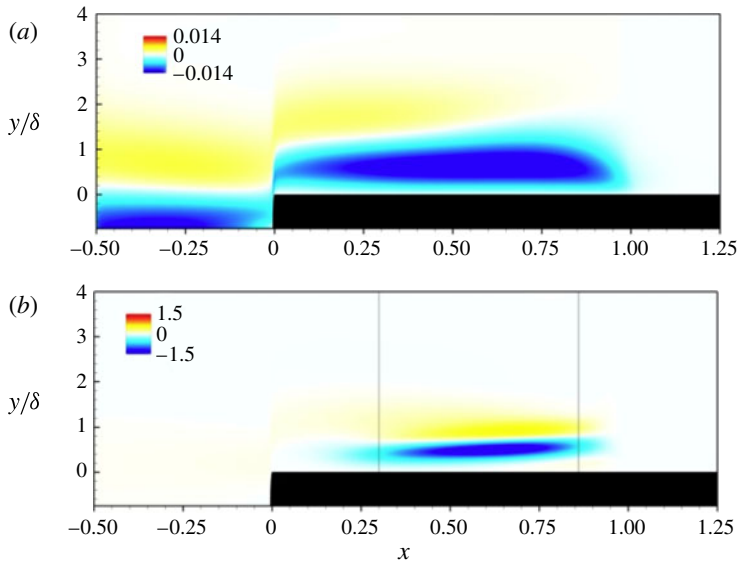

FIGURE 19. Sensitivity to steady forcing. Stream-wise component of the field $\delta^2/\sigma^2\mathbf{\nabla}_F\sigma^2$ for the (*a*) LU and (*b*) TS perturbations.

$\delta\sigma^2 \sim 1.5\sigma^2\epsilon$ showing that a small steady forcing may have a dramatic effect on the development of TS perturbations. At the same time, the energy of the LU perturbations would decrease as $\delta\sigma^2 \sim 0.01\sigma^2\epsilon$.

Finally, the sensitivity fields to wall-normal blowing/suction is depicted in figure 18(*b*). The tangential components are not shown since their effect is negligible. At a first look this may seem inconsistent with the results obtained for the sensitivity to steady forcing where modification of the streamwise components is dominant.

However, in boundary layer flows, wall-normal blowing and suction induce efficiently mainly variations of the streamwise component of the base flow. The result for the TS perturbation is displayed by the solid line in figure 18(*b*). It indicates that suction around $x = 0.5$ should be applied to reduce the perturbation energy. For the LU perturbation the localization of the blowing is less pronounced. Since the LU perturbation is also much less sensitive, suction distributed on the whole flat plate should be chosen to achieve a significant reduction of the perturbation energy growth. Finally we note that a peak is reached around $x = 0.3$, i.e. further upstream than in the case of steady forcing (compare with figure 18*a*).

5. Concluding remarks

A theoretical formulation to study the base-flow sensitivity of fluid problems characterized by significant non-modal amplification of linear perturbations is proposed. These base-flow variations can be seen as defects from ideal configurations as well as the result of passive manipulation of the flow. Using a variational technique, we have derived the analytical expression for the gradient of the resolvent norm of the system with respect to the base-flow modifications. We have shown that this gradient depends on the combination of the optimal forcing and the optimal response, in analogy to the sensitivity of the eigenvalue that is largest in the overlap region between direct and adjoint eigenmodes (Chomaz 2005). Therefore, in parallel with the concept of wavemaker introduced for globally unstable flows (hydrodynamic oscillators), we consider the region in space where the largest amplification of external noise of given frequency is occurring in globally stable systems. This is located within the region of largest sensitivity to base-flow modifications.

Results are presented for the Blasius boundary layer, a classic example of a noise amplifier where the different instability mechanisms of shear flows are at work. We investigate how the sensitivity of the resolvent norm varies for the two sources of non-normality present, component-wise (LU) and convective (TS). The results show that very weak modifications of the base flow can have a significant impact on the TS waves, easily leading to more unstable flows. Conversely, the sensitivity of elongated perturbations exploiting the LU mechanism is weaker, almost independent of the Reynolds number and larger further up in the boundary layer and upstream of it. When imposing divergence-free distortions we observe that modification of the streamwise component of the base flow is dominant, whereas variations of the wall-normal velocity component has little impact on either instability. The findings presented can be explained just by examining the gradient of the resolvent norm with respect to base-flow modifications in the limit of small spanwise wavenumbers and low frequencies. Finally, we considered also the effect of steady forcing and wall blowing/suction on the instability (both acting via a base-flow modification) to demonstrate the potential of the current approach for the design of passive control strategies.

For the case of boundary layer flows, where two distinct instability mechanisms are at work, it is relevant to examine how variations of the base flow that are optimal for one type of disturbances can affect the other. To this end, we have considered modifications of the base-flow which are optimal to enhance/reduce the LU or the TS mechanism and studied the resulting flow behaviour in the wavenumber plane. Our results, not shown here, show that variation of the base flow reducing the LU amplification can easily lead to increased amplification of TS waves. Conversely, weak variations of the shear layer close to the wall can greatly affect the TS amplification

while having no effect on the LU (as deduced by the largest magnitude of the sensitivity to TS). Note indeed that it is necessary to scan the entire parameter space to be sure that a distortion-stabilizing perturbation at some (ω_0, β_0) did not produce an amplification increase in a different region in wavenumber space.

We examined the analytical expression of the sensitivity to gain physical understanding on the instability mechanisms and the potential that variations of the base flow may have. The sensitivity gradient alone provides information on the effect of small-amplitude base-flow modifications on the non-modal behaviour. However, it is important to note that the gradient can also be used to determine the change in the base-flow velocity profile of specified finite magnitude that has the largest effect on the singular values of the system, see Bottaro *et al.* (2003) for the corresponding modal analysis.

In conclusion, the analysis presented here is relevant for all open flows which are globally stable, such as spatially evolving incompressible boundary layers forming on aerofoils. The present paper introduces, therefore, sensitivity analysis tools for noise amplifiers. Note finally that in our approach we target directly the non-modal flow behaviour and the formulation can be extended to design active control strategies aimed at the flow non-modal disturbance growth. This could be a viable alternative in the case of non-parallel flows with large streamwise non-normality.

Appendix. Sensitivity analysis in the time domain

The derivation reported above for the forced problem can be extended to consider the largest transient growth in time of an optimal initial condition. In this case, the largest singular value of the linear evolution operator is the target of the sensitivity analysis. The main steps and the final result are briefly outlined here.

The relation between the optimal initial condition $\boldsymbol{u}_{in}(t=0)$ and the response $\boldsymbol{u}_{out}(t_f)$ at given time $t=t_f$ can be formally written

$$\boldsymbol{u}_{out} = \mathscr{T}(t_f, \boldsymbol{U})\boldsymbol{u}_{in}, \quad \mathscr{T} = \mathscr{P}^{\mathrm{T}}\mathscr{E}(t_f, \boldsymbol{U})\mathscr{P}, \quad \mathscr{E} = \exp(t_f\mathscr{L}(\boldsymbol{U})). \quad (A\,1)$$

The evolution operator $\mathscr{T}$ is defined as the matrix exponential of the stability operator $\mathscr{L}$. The optimal initial condition is defined as the eigenfunction associated with the largest eigenvalue of the symmetric operator

$$\mathscr{T}^{\dagger}\mathscr{T}\boldsymbol{u}_{in} = \lambda^2\boldsymbol{u}_{in}, \quad (A\,2)$$

and it maximizes the gain $G(\boldsymbol{u}_{in}) = ((\boldsymbol{u}_{out}, \boldsymbol{u}_{out})/(\boldsymbol{u}_{in}, \boldsymbol{u}_{in}))$. Defining a Lagrangian in the same way as described above, targeting modification of the largest singular value of the evolution operator,

$$\mathscr{K}_{\tau} = \lambda^2 - (\boldsymbol{q}_{\tau}^{\dagger}, \boldsymbol{u}_{out} - \mathscr{T}\boldsymbol{u}_{in}) - (\boldsymbol{a}_{\tau}^{\dagger}, \boldsymbol{a}_{\tau} - \mathscr{T}^{\dagger}\boldsymbol{u}_{out}) - (\boldsymbol{f}_{\tau}^{\dagger}, \lambda^2\boldsymbol{u}_{in} - \boldsymbol{a}_{\tau}), \quad (A\,3)$$

the sensitivity function $\nabla_U\lambda^2$ is, in analogy to the case of the resolvent norm,

$$\nabla_U\lambda^2 = 2\lambda^2\mathrm{Re}\{(\nabla\boldsymbol{u}_{in})\,\boldsymbol{u}_{out}^* - (\nabla\boldsymbol{u}_{out})^H\boldsymbol{u}_{in}\}, \quad (A\,4)$$

where the optimal initial condition is normalized so that $(\boldsymbol{u}_{in}, \boldsymbol{u}_{in}) = 1$ and the response at final time is $(\boldsymbol{u}_{out}, \boldsymbol{u}_{out}) = \lambda^2$.

REFERENCES

ÅKERVIK, E., EHRENSTEIN, U., GALLAIRE, F. G. & HENNINGSON, D. S. 2008 Two-dimensional global stability measures of the flat plate boundary-layer flow. *Eur. J. Mech. (B/Fluids)* **27**, 501–513.

ALIZARD, F., CHERUBINI, S. & ROBINET, J.-C. 2009 Sensitivity and optimal forcing response in separated boundary layer flows. *Phys. Fluids* **21**, 064108.

BARKLEY, D., BLACKBURN, H. M. & SHERWIN, S. J. 2008 Direct optimal growth analysis for time steppers. *Intl J. Numer. Meth. Fluids* **57**, 1435–1458.

BLACKBURN, H. M., BARKLEY, D. & SHERWIN, S. J. 2008 Convective instability and transient growth in flow over a backward-facing step. *J. Fluid Mech.* **608**, 271–304.

BOTTARO, A., CORBETT, P. & LUCHINI, P. 2003 The effect of base flow variationon flow stability. *J. Fluid Mech.* **476**, 293–302.

BRANDT, L., SCHLATTER, P. & HENNINGSON, D. S. 2004 Transition in boundary layers subject to free stream turbulence. *J. Fluid Mech.* **517**, 167–198.

BUTLER, K. M. & FARRELL, B. F. 1992 Three-dimensional optimal perturbations in viscous shear flow. *Phys. Fluids* A **4**, 1637–1650.

CATHALIFAUD, P. & LUCHINI, P. 2000 Algebraic growth in boundary layers: optimal control by blowing and suction at the wall. *Eur. J. Mech. (B/Fluids)* **19**, 469–490.

CHOMAZ, J.-M. 2005 Global instabilities in spatially developing flows: non-normality and nonlinearity. *Annu. Rev. Fluid Mech.* **37**, 357–392.

CHOMAZ, J. M., HUERRE, P. & REDEKOPP, L. G. 1991 A frequency selection criterion in spatially developing flows. *Stud. Appl. Maths* **84**, 119–144.

CORBETT, P. & BOTTARO, A. 2000 Optimal perturbations for boundary layers subject to stream-wise pressure gradient. *Phys. Fluids* **12** (1), 120–130.

FARRELL, B. F. 1988 Optimal excitation of perturbations in viscous shear flow. *Phys. Fluids* **31**, 2093–2102.

FARRELL, B. F. & IOANNOU, P. J. 1996 Generalized stability theory. Part I: autonomous operators. Part II: nonautonomous operators. *J. Atmos. Sci.* **53**, 2025–2053.

GAVARINI, I., BOTTARO, A. & NIEUWSTADT, F. T. M. 2004 The initial stage of transition in pipe flow: role of optimal base-flow distortions. *J. Fluid Mech.* **517**, 131–165.

GIANNETTI, F. & LUCHINI, P. 2007 Structtural sensitivity of the first instability of the cylinder wake. *J. Fluid Mech.* **581**, 167–197.

GROSCH, C. E. & SALWEN, H. 1978 The continuous spectrum of the Orr–Sommerfeld equation. Part 1. The spectrum and the eigenfunctions. *J. Fluid Mech.* **87**, 33–54.

HUERRE, P. & ROSSI, M. 1998 Hydrodynamic instabilities in open flows. In *Hydrodynamic and Nonlinear Instabilities* (ed. C. Godrèche & P. Manneville). pp. 81–294. Cambridge University Press.

JOVANOVIC, M. R. & BAMIEH, B. 2005 Componentwise energy amplification in channel flows. *J. Fluid Mech.* **534**, 145–183.

LANDAHL, M. T. 1980 A note on an algebraic instability of inviscid parallel shear flows. *J. Fluid Mech.* **98**, 243–251.

MARQUET, O., LOMBARDI, M., CHOMAZ, J. -M., SIPP, D. & JACQUIN, L. 2009 Direct and adjoint global modes of a recirculation bubble: lift-up and convective non-normalities. *J. Fluid Mech.* **622**, 1–21.

MARQUET, O., SIPP, D. & JACQUIN, L. 2008 Sensitivity analysis and passive control of cylinder flow. *J. Fluid Mech.* **615**, 221–252.

MONOKROUSOS, A., ÅKERVIK, E., BRANDT, L. & HENNINGSON, D. S. 2010 Global three-dimensional optimal disturbances in the Blasius boundary-layer flow using time steppers. *J. Fluid Mech.* **650**, 181–214.

PRALITS, J. O., AIRIAU, C., HANIFI, A. & HENNINGSON, D. 2000 Sensitivity analysis using adjoint parabolized stability equations for compressible flows. *Flow Turbul. Combust.* **65**, 321–346.

PRALITS, J. O., BRANDT, L. & GIANNETTI, F. 2010 Instability and sensitivity of the ow around a rotating circular cylinder. *J. Fluid Mech.* **650**, 513–536.

REDDY, S. C. & HENNINGSON, D. S. 1993 Energy growth in viscous channel flows. *J. Fluid Mech.* **252**, 209–238.

SCHMID, P. J. & HENNINGSON, D. S. 2001 *Stability and Transition in Shear Flows*. Springer.

SCHRADER, L.-U., BRANDT, L., MAVRIPLIS, C. & HENNINGSON, D. S. 2010 Receptivity to free stream vorticity of flow past a flat plate with elliptic leading edge. *J. Fluid Mech.* **653**, 245–271.

SIPP, D., MARQUET, O., MELIGA, P. & BARBAGALLO, A. 2010 Dynamics and control of global instabilities in open flows: a linearized approach. *Appl. Mech. Rev.* **63**, 030801.

WEIDEMAN, J. A. C. & REDDY, S. C. 2000 A MATLAB differentiation matrix suite. *ACM Trans. Math. Softw.* **26** (4), 465–519.

ZAKI, T. A. & DURBIN, P. A. 2005 Mode interaction and the bypass route to transition. *J. Fluid Mech.* **531**, 85–111.

ZUCCHER, S., LUCHINI, P. & BOTTARO, A. 2004 Algebraic growth in a Blasius boundary layer: optimal and robust control by mean suction in the nonlinear regime. *J. Fluid Mech.* **513**, 135–160.